International Journal of Pharmaceutics 646 (2023) 123473

Contents lists available at ScienceDirect

International Journal of Pharmaceutics

journal homepage: www.elsevier.com/locate/ijpharm

Polyenylphosphatidylcholine as bioactive excipient in tablets for the treatment of liver fibrosis

Ivo Skorup [a,1], Gina Valentino [a,1], Simone Aleandri [a], Rita Gelli [b], Aymar Abel Ganguin [a], Eric Felli [c,d], Sonia Emilia Selicean [c,d], Rosanne Angela Marxer [a], Sarah Teworte [a], Ana Lucić [a], Jordi Gracia-Sancho [c,d,e], Annalisa Berzigotti [c,d], Francesca Ridi [b], Paola Luciani [a,*]

[a] Department of Chemistry, Biochemistry and Pharmaceutical Sciences, University of Bern, Bern, Switzerland
[b] Department of Chemistry "Ugo Schiff" and CSGI, University of Florence, Sesto Fiorentino, Florence, Italy
[c] Department of Visceral Surgery and Medicine, Inselspital, Bern University Hospital, University of Bern, Bern, Switzerland
[d] Department for BioMedical Research, Hepatology, University of Bern, Bern, Switzerland
[e] Liver Vascular Biology Research Group, CIBEREHD, IDIBAPS Research Institute, Barcelona, Spain

ARTICLE INFO

Keywords:
Phospholipids
Liver fibrosis
Lipid-based tablets
Hepatic stellate cells

ABSTRACT

Liver fibrosis is a condition characterized by the accumulation of extracellular matrix (ECM) arising from the myofibroblastic transdifferentiation of hepatic stellate cells (HSCs) occurring as the natural response to liver damage. To date, no pharmacological treatments have been specifically approved for liver fibrosis. We recently reported a beneficial effect of polyenylphosphatidylcholines (PPCs)-rich formulations in reverting fibrogenic features of HSCs. However, unsaturated phospholipids' properties pose a constant challenge to the development of tablets as preferred patient-centric dosage form. Profiting from the advantageous physical properties of the PPCs-rich Soluthin® S 80 M, we developed a tablet formulation incorporating 70% w/w of this bioactive lipid. Tablets were characterized via X-ray powder diffraction, thermogravimetry, and Raman confocal imaging, and passed the major compendial requirements. To mimic physiological absorption after oral intake, phospholipids extracted from tablets were reconstituted as protein-free chylomicron (PFC)-like emulsions and tested on the fibrogenic human HSC line LX-2 and on primary cirrhotic rat hepatic stellate cells (PRHSC). Lipids extracted from tablets and reconstituted in buffer or as PFC-like emulsions exerted the same antifibrotic effect on both activated LX-2 and PRHSCs as observed with plain S 80 M liposomes, showing that the manufacturing process did not interfere with the bioactivity of PPCs.

1. Introduction

Natural phospholipids, extracted from soybean or egg, are frequently used as excipients in the development of new pharmaceutical products. These phospholipids, characterized by a low batch-to-batch variability, are derived from renewable sources, produced with ecologically sustainable procedures, and they are available on a larger scale at a relatively low cost compared to synthetic ones, which have found application in only a few pharmaceutical products (van Hoogevest and Wendel, 2014; Varganova et al., 2019).

Soybean extracts of polyenylphosphatidylcholines (PPCs), belonging to the wide family of essential phospholipids (EPLs), have already been formulated in dietary supplements for the support therapy of chronic liver diseases (Gundermann et al., 2016). Remarkably, these "generally recognized as safe" (GRAS) lipids do not exert their function only as an excipient, but also as a bioactive component, as demonstrated in previous studies (Varganova et al., 2019; Gundermann et al., 2016). Alone or combined with other hepatoprotective compounds such as silymarin, EPLs are commonly used in some countries, like Russia and Poland, for patients suffering from non-alcoholic fatty liver diseases (NAFLD) and steatohepatitis (NASH), (Gundermann, 1993; Maev, 2019) due to their antioxidant and anti-inflammatory effects, although their mechanism of action is not fully understood yet.

EPLs are commercially available as hard or soft capsules. Both pharmaceutical dosage forms are favored by EPLs' suitability as a liquid filler due to phospholipids' physicochemical properties (Grune and

* Corresponding author.
E-mail address: paola.luciani@unibe.ch (P. Luciani).
[1] These authors contributed equally.

https://doi.org/10.1016/j.ijpharm.2023.123473
Received 23 April 2023; Received in revised form 24 August 2023; Accepted 30 September 2023
Available online 1 October 2023

Bunjes, 2020). Compared to soft capsules, hard gelatine capsules offer advantages for liquid and semi-solid formulations, as they do not require additional plasticizers and can be filled at higher temperatures (Grune and Bunjes, 2020). While the lipid amount can reach up to 100% in soft and hard capsule systems, the tableting process significantly reduces the lipid amount per dosage unit (Hauss, 2007; Kuentz, 2012). Physical integrity and mechanical strength of conventional compressed tablets are often compromised by using lipid excipients (Hauss, 2007). At ambient temperature, mono- and polyunsaturated lipids are in a liquid crystalline state (van Hoogevest and Wendel, 2014), and storage conditions and handling require strict humidity and/or temperature control together with oxidation prevention precautions (van Hoogevest, 2017). Only with a careful fine-tuning of the formulation composition can a consistent compendial quality of the manufactured tablets be achieved, as recently emphasized in the case study by Koch *et al.* on the use of lipid excipients to produce lipid tablets with optimal properties (Koch et al., 2023).

Compressing tablets majorly composed of unsaturated, bioactive phospholipids – the recommended daily dose of EPLs is between 1.05 and 1.80 g following oral intake, for instance (Gundermann, 1993; Gundermann et al., 2016) – may thus be considered a breakthrough in pharmaceutical manufacturing and NAFLD pharmacological management.

Recently, our group showed that PPC nanodispersions can revert activated, profibrogenic LX-2, immortalized human hepatic stellate cells (HSCs) to a quiescent-like status (Valentino et al., 2019). Specifically, we screened the antifibrotic effects of PPC liposomes, both in the presence and absence of silymarin, by using the fibrogenic human HSC line LX-2 cells. More recently, we identified the secreted protein acidic and rich in cysteine (SPARC), a matricellular protein, as one of the fibrogenesis-associated factors in extracellular vesicles (EVs) (Zivko et al., 2022). The direct treatment of LX-2 with two experimental antifibrotic drugs, elafibranor and obeticholic acid, increased the secreted SPARC in EVs (Zivko et al., 2023). However, the damaging drugs' effect on HSCs could be mitigated when formulating them with PPC. Proteomics and lipidomics profiling pointed out specific changes in LX-2 and LX-2-derived EVs, and biological assays indicated that the beneficial antifibrotic features of our PPC treatments can be transferred from the parent cells to the EVs (Zivko et al., 2023).

Among the several PPC-rich phospholipids commercially available, Soluthin® S 80 M, a magnesium chloride lecithin analogue of the phospholipid S 80, (Valentino et al., 2019) shows flow properties remarkably suitable for tableting. Here, we blended S 80 M with microcrystalline cellulose (MCC, filler), magnesium aluminometasilicate (oils adsorbent), and sodium croscarmellose (disintegrant in direct compression), generating a powder mixture that could be directly compressed into high-quality tablets complying with the compendial requirements (Ph. Eur. 11.0, 0478, 01/2023). The amount of water absorbed by the tablets and by their components after equilibrating at relative humidity (RH) 75% was estimated by thermogravimetric analyses. Via X-ray powder diffraction (XRPD) performed before and after tableting, we assessed if and how the compression step affected the bulk property of the powder and its crystalline state. Raman imaging was also employed to evaluate a homogeneous distribution of S 80 M in the tablet.

Finally, we investigated whether tableting PPCs could affect the antifibrotic bioactivity of S 80 M. PPCs were quantitatively extracted from tablets, reconstituted in aqueous solvent or in chylomicron-like emulsions mimicking the lipid uptake from the small intestine to the liver, and tested on activated human HSCs immortalized cell model (LX-2) and on primary hepatic stellate cells (PRHSC) obtained from cirrhotic rats to validate the ability of these formulations to revert fibrotic features not only in a cell line but also in primary cells.

2. Materials and methods

2.1. Materials

Soluthin® S 80 M (S 80 M, soybean phospholipid 80% complexed with $MgCl_2$), and 1,2-dioleoyl-*sn*-glycero-3-phosphocholine (DOPC) were a kind gift from Lipoid GmbH (Ludwigshafen, Germany). The LX-2 cells immortalized human HSC line (RRID: CVCL_5792) were purchased from Merck Millipore (Darmstadt, Germany). LX-2 cells originate from LX-1 cells that were obtained from isolated human HSCs and immortalized with Symian virus 40 (SV40) large T antigen that are grown in 10% foetal bovine serum (FBS) by selecting a single clone subline from the outgrowth able to be cultured in low FBS concentration (1%) and are usually cultured in 2% FBS. (Xu, 2005) Dulbecco's Modified Eagle Medium (DMEM-HG, 4.5 g/L glucose, with phenol red and pyruvate, no glutamine), 4-(2-hydroxyethyl) piperazine-1-ethanesulfonic acid sodium (HEPES) solution, DMSO (dimethylsulphoxide), 4′,6-diamidino-2-phenylindole (DAPI), Roti®-Histofix 4% (acid-free, pH 7.4, % w/v phosphate-buffered formaldehyde solution) were purchased from Carl Roth (Arlesheim, Switzerland). Iscove's Modified Dulbecco's Medium (with phenol red and L-glutamine), phosphate buffer saline (PBS) (pH 7.4, without Ca/Mg), L-Glutamine, Penicillin-Streptomycin, microcrystalline cellulose (MCC), hydrochloric acid (HCl), sodium hydroxide (NaOH), chloroform ($CHCl_3$), ethanol (EtOH), trifluoroacetic acid (TFA), isopropanol, acetone, methanol (MeOH), acetonitrile (ACN), TRIzol™ reagent, RNAse-free water were purchased from Fisher Scientific (Reinach, Switzerland). Foetal bovine serum (FBS), Accutase®, Cell Counting Kit-8 (CCK-8), 1,6-Diphenyl-1,3,5-hexatriene (DPH), N,N,N-trimethyl-4-(6-phenyl-1,3,5-hexatrien-1-yl)-phenyl-ammonium-p-toluolsulfonate (TMA-DPH), cholesterol, Oil Red O (ORO; 0.5% w/v in propylene glycol), collagen type I (from rat tail), triethyl citrate, and glycogen were bought from Sigma Aldrich (Buchs, Switzerland). Myritol® 318 triglycerides (produced by BASF Personal Care and Nutrition GmbH, Monheim am Rhein, Germany) were obtained from Impag (Zürich, Switzerland). Cell culture plates and flasks were from Sarstedt (Nümbrecht, Germany), TPP (Trasadingen, Switzerland) and Nunc (Roskilde, Denmark). ROS-ID® Total ROS/Superoxide detection kit was from Enzo Life Science (Lausen, Switzerland).

Neusilin® US2 (Fuji Chemical Industries Co., Ltd., Toyoma, Japan) was a kind gift from IMCD (Zürich, Switzerland). Primellose® was a kind gift from DFE Pharma (Goch, Germany). The enteric methacrylic acid copolymer Eudragit® L100-55 was a kind gift from Evonik (Essen, Germany).

2.2. Tablets preparation

70% (w/w) of S 80 M was mixed by dry granulation with 23% (w/w) MCC, 2% (w/w) Neusilin, and 5% (w/w) Primellose®. First, S 80 M was ground in a mortar with a pestle and blended with the excipients until a homogenous mixture was obtained. To ameliorate the mixture's homogeneity, a Turbula T 2F 3D mixer (Willy A. Bachofen, Muttenz, Switzerland) was employed for 5 min. The mixture was sieved (1400 μm) into a plastic container into which nitrogen gas was flushed and the container was sealed and kept at + 4 °C until the compression. Tableting was carried out using a single punch press XP1 from Korsch (Berlin, Germany) and tablets were manually compressed using a 11 mm matrix and round concave stamps from Natoli Engineering Company (Saint Charles, MO, USA), with insertion and filling depths of 5 mm and 5.5 mm, respectively. Both powder mixing and tableting were performed in an air-conditioned room at + 15 °C. Tablets were kept at + 4 °C under inert nitrogen atmosphere.

2.3. Compendial powder quality tests

The mixture flow analysis was performed in accordance with the Ph. Eur. monographs 2.9.16. and 2.9.36 Edition 10. using an Erweka GTL

granules and powder flow tester (Langen, Germany) equipped with one hopper of 480 mL and a nozzle of 25 mm.

The bulk volume (V_0) of mixture was measured in a 100 mL measuring cylinder as well as the volume after 10 taps (V_{10}), 500 taps (V_{500}) and 1250 taps (V_{1250}) by means of an Erweka SVM 222 tapped density tester (Langen, Germany). Bulk and tapped densities were calculated as 25 g/V_0 and 25 g/V_{1250}, respectively. As indicated by Ph. Eur. 2.9.36, the compressibility index (CI) was calculated from the bulk and tapped densities using the following equation (Eq. (1)):

$$CI = 100 \times [(V_0 - V_{1250})/V_0] \quad (1)$$

While the Hausner ratio (HR) was calculated using the following formula (Eq. (2)):

$$HR = V_0/V_{1250} \quad (2)$$

Bulk and tapped densities were calculated using the following formula (Eq. (3),4)), where m stands for the exact mass of powder that the test was performed on (~25 g):

$$BD = V_0/m \quad (3)$$

$$TD = V_{1250}/m \quad (4)$$

2.4. Compendial tablets quality tests

Twenty tablets were randomly chosen from a population and weighed on an analytical balance (Kern ADB 200–4; Ballingen, Germany), and their mean mass was determined.

Approximately 6.5 g of tablets were weighed on an analytical balance and tested with Erweka TAR 120 tablet friability and abrasion tester (Langen, Germany) with a setting of 100 revolutions, with a defined velocity of 25 rpm, as prescribed by Ph. Eur. 2.9.7. Tablets were weighed again, and the mass difference calculated. Furthermore, 10 tablets were arbitrarily tested for hardness on Erweka TBH 125 tablet hardness tester (Langen, Germany), using a constant speed setting (2.3 mm/s). Maximum, minimum, and mean values were determined following Ph.Eur. 2.9.8.

2.5. Gastro-resistant coating of tablets

Compressed tablets were coated with the functional enteric coating Eudragit® L100-55, by modifying the manufacturer's dip-in protocol. The coating suspension was prepared by mixing solvents (acetone, isopropanol, ultrapure water, 30:46:4% w/w of total) to which triethyl citrate and Eudragit® were added (3.33:16.67 % w/w) gradually and stirred with Polytron® PT 2500 E (Kinematica, Malters, Switzerland) for about 1 h until the suspension did become transparent and homogenous. Tablets were manually inserted in the coating suspension for approx. 10 sec and then air-dried for 20–30 min and then reinserted 5 times to give layers of coating. Coated tablets were kept at + 4 °C under a nitrogen atmosphere.

2.6. Disintegration of gastro-resistant tablets

To check the targeted location of tablet disintegration, the gastro-resistant tablets were tested using the Automated Disintegration System G7962A from Agilent (Santa Clara, CA, USA). Experimental conditions were followed from Ph. Eur. 2.9.1, 5.17.1 and Tablets monography (Ph. Eur. 11.0, 0478, 01/2023) (medium temperature: 37 °C; medium volume: 900 mL; 6 tablets per test). Tablets were kept in the apparatus for 2 h in HCl 0.1 M without discs, transferred to phosphate buffer pH 6.8 (PB) with added discs and kept in PB buffer for 1 h.

2.7. Thermogravimetry (TGA)

The amount of water absorbed by the tablet and by the tablet's components upon equilibration at RH 75% was evaluated by thermogravimetry. The analyses were conducted using a Discovery SDT 650 from TA Instruments (New Castle, DE, USA). Samples were loaded in aluminum pans and heated from room temperature (RT) to 500 °C, at 10 °C/min, in N_2 atmosphere (flow 100 mL/min). The weight loss between RT and 150 °C was used to estimate the amount of water in the samples, which was calculated as the difference between the weight loss of the same sample equilibrated at RH 75% and that of the freeze-dried one. The equilibration process was carried out by placing small aliquots of powders or tablets in a hermetically closed chamber together with NaCl saturated solution, at + 4 °C, for one week. The freeze-drying process was conducted by freezing the samples in liquid N_2 (-196 °C) and lyophilizing them at −50 °C and 50 mTorr for 24 h (VirTis Benchtop freeze-dryer, Gardiner, NY, USA).

2.8. X-ray powder diffraction (XRPD)

XRPD analyses were carried out using a D8 Advance powder diffractometer from Bruker (Billerica, MA, USA) equipped with a Cu X-ray source (λ = 1.54 Å) working at 40 kV and 40 mA. Samples were ground with agate mortar and pestle and flattened on a Si low background sample holder. The diffraction patterns were collected in the 2θ range 3-50°, with an increment of 0.03°, a time *per* step of 0.3 s, and with a 0.6 mm slit.

2.9. Confocal Raman microscopy

Confocal Raman measurements were conducted on a Renishaw inVia™ Qontor™ confocal Raman microscope (Wotton-under-Edge, UK) equipped with a 785 nm laser, a front-illuminated CCD camera, and a research-grade Leica DM 2700 microscope. The spectra of the tablet's components were collected using a 20x objective (numerical aperture 0.40, working distance 1.15 mm) in the 200–3200 cm^{-1} range, a laser power of 10 mW, and an exposure time of 10 s with 5 accumulations. The tablet's chemical map was obtained with a 5x objective (numerical aperture 0.12, working distance 14 mm) using the StreamLine™ mode, which allows for the fast imaging of large sample areas. In this case, the laser power was 100 mW, the exposure time 15 s with 1 accumulation, and the Raman shifts range 680–1730 cm^{-1}. Four maps of 1.8 mm × 1.0 mm were collected (step along x: 20 μm, step along y: 14.2 μm), resulting in a total imaged area of 3.6 × 2.0 mm. The S 80 M distribution within the tablet was obtained considering the intensity at 1658 cm^{-1}, which is the maximum of a peak characteristic only of the lipid.

2.10. Preparation of protein-free chylomicrons (PFC)

PFC were prepared by modifying previously described emulsions (Mortimer, 1995). Briefly, 70% (w/w) S 80 M extracted from tablets, 3% (w/w) triglycerides from saturated fatty acids, 2 % (w/w) cholesterol, and 25% (w/w) DOPC were dissolved in 3:1 (v/v) ratio of methanol-chloroform. Solvents were evaporated under a stream of nitrogen before an overnight vacuum to eliminate residual solvent traces. The dried lipid mixture was dissolved in HEPES buffer (10 mM, pH 7.4) to reach 50 mM S 80 M and 18 mM DOPC concentration and sonicated for 20 min at 37 °C. Control emulsions without S 80 M (PFC) were also produced with 10% (w/w) triglycerides from saturated fatty acids, 6.7% (w/w) cholesterol, and 83.3% (w/w) DOPC and diluted to 18 mM DOPC concentration. PFC treatments were further diluted in a serum-free experimental cell culture medium (*vide infra*, **Section 2.13**) 1:10 to treat the cells to reach final S 80 M and DOPC concentrations of 5 mM of 1.8 mM, respectively.

2.11. S 80 M extraction from tablets

S 80 M from tablets was extracted by crushing them in the mortar and dissolving them in 1 mL of 3:1 (v/v) ratio of methanol-chloroform

solution. Samples were then vortexed (5 min) and sonicated (10 min) at 37 °C. Further centrifugation (10 min at 3400 g) allowed the separation of the supernatant containing lipids. The solution was left to rest in an upright position for 5 min. The extraction step was repeated four times until a clear supernatant was obtained. The organic solvents present in the supernatant were evaporated under an inert nitrogen gas and later under reduced pressure (12 h) to eliminate residual solvent traces. The dried lipids were kept dried for further experiments, reconstituted in methanol for HPLC-CAD lipid quantification (available in the Supplementary Data, **Figure S1**), or dissolved in HEPES buffer (10 mM, pH 7.4) to reach S 80 M 50 mM concentration for use on cells.

2.12. Cell culture and general information about cell experiments

LX-2 cells were grown at 37 °C in a 5% CO_2 humidified atmosphere in an LX-2 complete medium: DMEM-HG (4.5 g/L glucose, phenol red, no L-glutamine, pyruvate) supplemented with 1% *v/v* penicillin/streptomycin mixture (penicillin: 10′000 U/mL, streptomycin: 10′000 µg/mL), 1% *v/v* of L-glutamine (2 mM), and 2% *v/v* FBS. Subcultivation was performed with Accutase® at a cell confluency of about 80–90 % according to the manufacturer's instructions. LX-2 at passage 8 to 14 were used for cell experiments. LX-2 cell experimental medium was serum-free complete medium.

For experiments, LX-2 cells were seeded either in 24-well microtiter plates with 0.5 mL/well at a density of 50′000 cells/well, or in 96-well microtiter plates with 100 µL/well at a density of 12.500 cells/well, and cultured for 18 h at 37 °C, 5 % CO_2 to ~ 90 % confluency. Treatments were always performed with 0.5 mL/well for 24 well plates or 100 µL/well for 96 well plates at 37 °C, 5% CO_2.

Primary rat hepatic stellate cells (PRHSC) were isolated according to established protocols. (Fernandez-Iglesias et al., 2019) PRHSCs were isolated from livers of cirrhotic Sprague Dawley rats that were treated with thioacetamide (TAA) for 12 weeks. Animal experiments were approved by the Veterinary Office of the Canton of Bern, Switzerland, under the License n. BE 90 2021 and followed accepted guidelines and regulations. After isolation, cells were seeded on assay microplates and grown at 37 °C in a 5 % CO_2-humidified atmosphere for 7 days in a PRHSC complete medium. Iscove's Modified Dulbecco's Medium (IMDM; phenol red, L-glutamine,) was supplemented with a 1% *v/v* penicillin/streptomycin mixture (penicillin: 10′000 U/mL, streptomycin: 10′000 µg/mL) and 10% *v/v* FBS to obtain PRHSC complete medium. PRHSC cells were grown for 7 days, not passaged, and used for cell experiments. PRHSC cell experimental medium was serum-free complete medium.

For experiments, PRHSC were directly seeded either in 24-well microtiter plates with 0.5 mL/well at a density of 50′000 cells/well, or in 96-well microtiter plates with 100 µL/well at a density of 12′500 cells/well, and cultured 7 days at 37 °C, 5 % CO_2 to reach 70–90% confluency. Microtiter plates were pre-coated with 2.5% (v/v) collagen type I (from rat tail) solution in PBS for 1 h at RT, plates were washed with PBS once, and cells were seeded. Cells were washed and the medium was exchanged first at 24 h after seeding, and then every 48 h until Day 7. Treatments were always performed with 0.5 mL/well for 24 well plates or 100 µL/well for 96 well plates at 37 °C, 5% CO_2.

2.13. Direct treatment of LX-2 and PRHSC

For the LX-2 cells, the medium from seeded cells was discarded the day after cell seeding, and the cells were rinsed once with phosphate-buffered saline (PBS). Treatments of cells in microtiter plates were performed directly. Briefly, the formulations (liposomes, tablet extract in HEPES buffer, tablet extract reconstituted as PFC-like emulsions, and PFC-like emulsions) were mixed with the experimental medium without FBS to reach a total lipid concentration of 5 mM of S 80 M, or in case of the PFC-like emulsions, DOPC concentration of 1.8 mM, and cells were incubated at 37 °C in a 5% CO_2 humidified atmosphere with this solution for 24 h and assayed.

For the PRHSC, the day before the treatment (Day 7), the medium from seeded cells was discarded, and the cells were rinsed once with phosphate-buffered saline (PBS). Treatments of cells in microtiter plates were performed directly. Briefly, the formulations (liposomes, tablet extract in HEPES buffer, tablet extract reconstituted as PFC-like emulsions, and PFC-like emulsions) were mixed with the experimental medium without FBS to reach a total lipid concentration of 5 mM of S 80 M, or in case of the PFC-like emulsions, DOPC concentration of 1.8 mM, and cells were incubated with this solution for 24 h and assayed.

2.14. Analysis of lipid droplet content by ORO

After cell treatment, both LX-2 and PRHSC cells in 24-well plates were washed three times with PBS, fixed with 500 µL/well Roti®-Histofix 4% for 10 min at RT, and washed once with PBS. Cells were stained with a 0.5% w/v ORO solution in propylene glycol (500 µL/well) for 15 min at RT. ORO solution was carefully removed using a pipette and cells rinsed with PBS. Nuclei were then counterstained with a DAPI solution (3.6 µM) in PBS for 5 min at RT. Afterward, cells were rinsed with PBS. Fluorescence and phase contrast image acquisition was performed using a Nikon Ti2-E (Nikon Instruments, Melville, NY, USA) inverted microscope with 20x magnification. DAPI filter (λ_{ex} 360 nm, λ_{em} 460 nm), TxRed filter (λ_{ex} 560 nm, λ_{em} 645 nm) were used. The fluorescent binary area in the TxRed field was examined using the FIJI/ImageJ software. (Schindelin, 2012) Shortly, for each image, the qualitative interpretation of images was supplemented by quantification of fluorescence to have a transparent comparative purpose and confirm observed results. A fluorescent ORO relative intensity (FRI) was obtained by normalizing the fluorescent binary area (μm^2) in the fluorescent field to the number of objects (cell nuclei number) in the DAPI field.

2.15. Reactive oxygen species (ROS)

After treatments, both LX-2 and PRHSC cells in 96-well plates were washed with PBS (100 µL/well) and incubated with ROS-ID® Total ROS detection kit following the manufacturer's instruction.

Briefly, cells were washed and then incubated with ROS solution and the positive control (100 µL/well) for 2 h at 37 °C, 5% CO_2. After the incubation, the fluorescence was measured (λ_{ex} = 488 nm, λ_{em} = 520 nm) with an Infinite 200 Pro M−Nano plate reader (Tecan, Männedorf, Switzerland).

2.16. Cell proliferation assay (CCK-8)

The CCK-8 assay was used following the manufacturer's instructions. Briefly, after treatments (100 µL/well; 96 well plate), LX-2 and PRHSC cells were washed once with PBS. A volume of 90 µL of serum-free experimental medium and a volume of 10 µL of CCK-8 were added to each well. Cells were incubated for a further 2 h at 37 °C, 5% CO_2. Afterward, the absorbance was measured at 450 nm with an Infinite® 200 Pro M−Nano plate reader.

To calculate the cell metabolic activity in percent, the following equation was used (Equation (5)):

$$Cell\ metabolic\ activity\ (\%) = (OD\ sample / OD\ control) \times 100 \quad (5)$$

where "OD sample" refers to the optical density of the cells treated with the substances, and "OD control" is the cells exposed to serum-free experimental medium.

2.17. Motional order of the cell membrane in adherent cells

Stock solutions of the fluorescent probes DPH and TMA-DPH in DMSO were stored at −20 °C, and protected from light until use. Working solutions of DPH (8 µM) or TMA-DPH (5 µM) in PBS were prepared fresh before experiments from aliquots of the corresponding

fluorophore.

After cell treatments for 24 h, the adherent LX-2 and PRHSC cells were washed three times with PBS and 100 µL of DPH or TMA-DPH were added to each well of the 96-well plate (black bottom and wall). LX-2 cells were then further incubated at 37 °C, 5% CO_2 with DPH (2 h) or with TMA-DPH (10 min). After one PBS wash (100 µL/well), all the remaining solution was aspirated from the wells and fresh PBS was added to each well. The fluorescent anisotropy was measured with an Infinite 200 Pro F-Plex plate reader (Tecan, Männedorf, Switzerland) equipped with polarization filters (monochromator mode, $\lambda_{ex} = 360$ nm, $\lambda_{em} = 430$ nm) and calculated by applying the following formula (Equation (6)):

$$r = \frac{G \times I\| - I_{\perp}}{G \times I\| + 2I_{\perp}} \quad (6)$$

where the calibrated G factor (G) is 1.026, r is a calculated fluorescent anisotropy, $I_{\|}$ the parallel fluorescent intensity and $I_{\perp}$ the perpendicular fluorescent intensity.

2.18. qPCR gene expression analysis in LX-2 cells

After LX-2 cell treatment for 24 h, total RNA was isolated using TRIzol™ reagent following the manufacturer's protocol. Briefly, cells were lysed with TRIzol™ directly on the 24-well plate and transferred to 1.5 mL reaction tubes. A volume of chloroform equivalent to one-fifth of the total TRIzol™ volume was added to the samples. The tube was vortexed vigorously for 10 sec and was incubated at room temperature for 10 min, before being centrifuged for 20 min at 4 °C and 16′000 g. The upper phase was transferred to a new reaction tube, 1 µL glycogen and a volume of isopropanol equal to the volume of the upper phase were added and mixed well prior to the RNA precipitation on ice for 10 min. The RNA was pelleted by centrifugation for 10 min at 4 °C and 24′000 g. The supernatant was discarded, and the pellet was washed with 1 mL of 70% ethanol in RNAse-free water. The centrifugation was repeated twice and the final pellet was resuspended in RNAse-free water after air drying for a few minutes. The RNA concentration was measured with a NanoDrop (ThermoFisher, USA).

The isolated RNA was reverse-transcribed into cDNA. Briefly, 1000 ng of RNA were diluted in RNAse-free water and were incubated for 5 min at 65 °C after addition of 3 µL of a 150 ng/µL random hexamer (Microsynth, Switzerland). After 10 min incubation at RT, 13.5 µL of pre-mixed RT master mix was added (**Table S1**) and the samples were incubated for another 10 min at RT, followed by a 1 h incubation at 50 °C and 20 min incubation at 75 °C. RNAse-free water was added to reach a theoretical concentration of 8 ng/µL cDNA.

The primers (**Table S2**) were diluted in RNAse-free water to a primer pair solution of 2.5 µM of forward and reverse primer each. The remaining reagents (polymerase, nucleotides, buffer, fluorophore) for qPCR were in the Brilliant III Ultra-fast SYBR Green qPCR master mix (MM; Agilent, USA). The cDNA samples were measured in duplicate for each gene and cDNA dilution. A pipetting robot (Corbett Robotics, USA) was used to pipette the samples (3 µL cDNA, 7.5 µL 2x MM, 3 µL primer mix, 1.5 µL water). The samples were transferred to the qPCR analyzer centrifuge (Rotor-Gene Q 2Plex System, Qiagen, Germany) which performed 40 cycles of amplification at 95 °C and 60 °C, whereas the fluorescence was always measured at 60 °C (λ_{ex} 470 nm, λ_{em} 510 nm). After the 40 cycles, the melting curve of each sample was measured. The data were analyzed using the Rotor Gene Q version 2.3.5 software and Microsoft Excel 365. The qPCR data were analyzed using the delta-delta CT method. (Livak and Schmittgen, 2001) GAPDH was used as a reference gene.

2.19. Statistical tests and analysis

All experiments were performed in three independent replicates, and samples were freshly prepared, if not stated otherwise. Statistical analysis was carried out using GraphPad Prism version 9.5.1. Multiple comparisons between the groups were performed by an ordinary one-way ANOVA with *post-hoc* Tukey's multiple comparison analysis, respectively (statistical significance note as **** $p < 0.0001$, *** $p < 0.001$, ** $p < 0.01$, *$p < 0.05$). If not stated otherwise, the data are presented as mean ± S.D. (standard deviation calculated from independent samples). qPCR data is presented as mean ± S.E.M. (standard error of the mean).

3. Results and discussion

3.1. Compendial quality assays

In the present work, a soybean-derived phospholipid complexed with $MgCl_2$ (Soluthin® S 80 M) was formulated at a high percentage in tablets.

One of the most challenging aspects of developing an EPL-based tablet is the high lipid percentage needed to reach the daily hepatoprotective dose, reported to be 1.05–1.80 g (Gundermann, 1993; Gundermann et al., 2016). We aimed to incorporate the highest mass of S 80 M that would still ensure that compendial requirements could be met. We could incorporate 70% (w/w) soy phospholipid via dry granulation due to the physicochemical properties of PPC with low melting points. (van Hoogevest and Wendel, 2014; Chapman and Collin, 1965) Considering the demanding nature of the EPL formulation, the choice of excipients was of critical importance. MCC (23%, w/w) was chosen as a classical filler, binder, and anti-caking agent. Its plasticity enables efficient binding to other materials, especially poorly tabletable active pharmaceutical ingredients. (Thoorens et al., 2014; Trache, 2016) Primellose® (5%, w/w), croscarmellose sodium, is an absorbent hydrophilic but insoluble material with exceptional swelling and wicking properties, as such used as a disintegrant. (Kapoor et al., 2020) Neusilin® was added as an oil adsorbent due to its large surface area and for its ability to stabilize the mixture, improve the powder flow, and thus achieve a direct lipid tablet compression. (Tan et al., 2013; Hentzschel et al., 2011; Chakraborty et al., 2010) A preliminary design-of-experiment (DoE) formulation screening study, based on serendipity formulation, with a low percentage of soy phospholipid, did not yield any completely satisfying formulation. The highest-lipid content formulation from DoE, which was acceptable according to our criteria, was chosen and manually optimized for different components and quantities to obtain the tested one.

As shown in Table 1, the measured bulk and tapped density were 0.58 g/mL and 0.66 g/mL, respectively. The resulting Hausner's ratio (HR) and compressibility index (CI), used as indirect methods to estimate the flow properties, confirmed the good flow character of the powder, the second-best category in the scale of flowability reported in Ph. Eur. 2.9.36 (Ph. Eur. 11.0, 0478, 01/2023). The obtained HR and CI values were similar to those obtained in the study from Kolbina *et al.* (Kolbina et al., 2017) (CI 12.64 ± 1.21 and HR 1.15 ± 0.02), where saturated phosphatidylcholine (SPC) was formulated as a matrix for extended release dosage form.

The measured powder flow was 28.0 g/s, a value in agreement with good flow properties assessed by HR and CI evaluation. Based on these findings, this powder mixture was found to be suitable to be tabletted.

The ensuing powder mixture was compressed into tablets, which

Table 1
Powders' mixture properties. Mean ± S.D. (n = 3).

Property	Experimental values
Powder Flow	28.0 ± 4.2 g/s
Bulk density	0.5787 ± 0.0085 g/mL
Tapped density	0.6598 ± 0.0010 g/mL
Hausner Ratio	1.14 ± 0.02 – Good flow
Compressibility Index	12.30 ± 1.16 – Good flow

were subsequently analyzed following Ph. Eur. tests.The obtained friability of the tablets was low (0.09%, Table 2), mirroring the good mechanical properties of our solid dosage form together with shape and mass conservation, of pivotal importance especially during processes imminently after production, such as packaging, transportation, and use. Despite the softness of the excipients, the hardness of the tablets was 21.80 N, with an entire range going from 12 up to 41 N.

The Ph. Eur. disintegration test was carried out to determine the speed at which the tablet breaks down into smaller particles, allowing for a greater surface area and absorption of the phospholipid in the small intestine. Uncoated tablets fully disintegrated after less than 1 h and evidently did not comply with the pharmacopoeial gastro-resistance requirement of at least 2 h in HCl 0.1 M. Considered that EPLs' absorption and uptake occur with other lipids *via* retinyl esters and chylomicrons, starting from the small intestine, (Porter and Charman, 1997; Tso and Balint, 1986; Nayak et al., 2001) to avoid the disintegration and release of tablets in the stomach, the choice was to provide the tablets with a gastro-resistant coating to modulate their release. We manually dip-coated tablets as proof of principle, and disintegration tests were performed again to verify the efficiency of the coating layer. Coated tablets did not disintegrate in HCl 0.1 M for 2 h and did not display any structural damage. After their transfer to PB pH 6.8, complete disintegration occurred within the prescribed 1 h (**Figure S2**). We could thus demonstrate that with enteric coating we can modulate tablet disaggregation in the small intestine compartment as desired. Lastly, we performed a dissolution test of S 80 M tablets in PB pH 6.8 to verify that PPCs are released from the tablets in a simulated intestinal fluid (**Figure S3**).

3.2. Thermogravimetry

The hygroscopicity of the tablets and their components was assessed by means of TGA. Aliquots of samples were either freeze-dried or equilibrated at RH 75% (see the Materials and Methods section for further details), in order to quantify water absorption upon incubation in a humid environment. For TGA analysis, the samples were heated at 10 °C/min, and their weight loss as a function of temperature was monitored (Fig. 1).

The difference between the weight loss from RT to 150 °C of each sample, either freeze-dried or equilibrated at RH 75%, was taken as an indication of the amount of water present in the sample due to equilibration at RH 75%. The results given in Table 3 reveal that the lipid S 80 M is remarkably hygroscopic, as expected, since after equilibration at RH 75% it consists of 19 ± 3% w/w of water. MCC is the least hygroscopic component of the formulation, while the other excipients and both the powder mixture and the uncoated tablet display a water % ranging from ~ 14% to 17%.

3.3. (XRPD and Raman microscopy

The samples were characterized by means of XRPD, with the goal of understanding if the water uptake or the tableting process would impact the crystallinity. The diffraction patterns of the tablets' components are given in Fig. 2a-d. S 80 M displays sharp diffraction peaks at low angles, which reveal its liquid crystalline nature. The excipients are characterized by broad peaks that are diagnostic of a low degree of crystallinity, as expected given their polymeric nature. The patterns reveal that no significant difference between the freeze-dried and the equilibrated at RH 75% samples is observed, except for small variations in the S 80 M peaks intensity and position which can be attributed to the different amounts of water present in the samples: it is well known that the number of water molecules per phosphatidylcholines has an influence on their diffraction pattern. (Sautot, 2011).

The XRPD pattern of the sample S 80 M 70% equilibrated at RH 75% before and after tableting is given in Fig. 2f. Both samples show the narrow and intense peaks of S 80 M at low 2θ, together with broader signals at higher angles due to MCC and Primellose®. No differences were observed between the pattern of the tablet and the powder mixture, suggesting that the compression occurring during the tableting procedure does not influence the crystallinity of the formulation components. Such patterns refer to samples equilibrated at RH 75%, but the same considerations can be drawn for the freeze-dried samples, whose diffractograms are shown in Fig. 2e.

Kolbina *et al.* published similar findings, showing that after producing and characterizing matrices extruded from hydrogenated soybean phosphatidylcholine (HSPC), a change in HSPC's crystallinity was not observed. (Kolbina et al., 2019).

The distribution of the lipid within the tablet was analysed with confocal Raman mapping. We initially collected the Raman spectra of the different components constituting the formulation, which are shown in Fig. 3a. S 80 M shows a variety of signals in its spectrum, which are consistent with stretching and bending modes of vibration of phosphatidylcholines. (Pence and Mahadevan-Jansen, 2016) The spectra of MCC and Primellose® are similar to each other, which is reasonable considering that the two polymers derive from cellulose; the sharper peaks of MCC might be related to its more crystalline nature (see Fig. 2). Neusilin®, on the other hand, shows very weak and broad signals. The lack of distinctive peaks is consistent with its chemical nature, being a synthetic amorphous form of magnesium aluminometasilicate, and is in agreement with literature reports. (Azad et al., 2018).

To perform a Raman mapping and to discriminate between the components of a multi-phase sample it is fundamental to identify regions where no overlay between the signals of the different components are present: to our purposes, the peak at 1658 cm^{-1} of S 80 M, which corresponds to C = C stretching of unsaturated fatty acids, (Kochan, 2016) is particularly well suited to observe the distribution of this component within the tablet, since MCC, Primellose® and Neusilin® do not display any signal in this region. Therefore, we analysed a large area of the tablet (3.6 × 2.0 mm) collecting a white light image (Fig. 3b) in which the S 80 M distribution was obtained by observing in each pixel the intensity of the Raman spectrum at 1658 cm^{-1} (Fig. 3c). The lipid appears homogeneously distributed within the tablet on the length scale of tens of μm, as only domains of hundreds of μm can be observed. S 80 M−rich regions correlate with the yellowish areas visible in the white light image (Fig. 3b).

3.4. Modulation of LX-2 cell phenotype indicating antifibrogenic effects

Solid dosage forms cannot be tested as such on cells. Therefore, we decided to extract the phospholipids from tablets using the Bligh-Dyer method (Bligh and Dyer, 1959) and to reconstitute the lipids in a buffer. The efficiency of the extraction process of the lipids from the other excipients was assessed via HPLC-CAD, revealing 102.8% ± 2.7 lipid content recovery (**Figure S1**).

For a better understanding and comparison of the *in vitro* antifibrotic effect of S 80 M extracted from tablets, control treatments of S 80 M liposomes were produced via the film hydration method and extrusion through polycarbonate membranes as previously reported (Figure S4) (Valentino et al., 2019; Rahnfeld et al., 2018). To simulate a more physiologically relevant lipid transport method, extracted S 80 M from tablets was also reconstituted as a PFC-like emulsion (Porter and

Table 2
Tablets' properties measured according to Ph.Eur. 11. Mean ± S.D. (n = 3).

Property	Experimental Values
Mass	0.2950 g ± 0.0151
Friability	0.09 % ± 0.04
Minimum Hardness	12 N
Maximum Hardness	41 N
Mean Hardness	21.80 N ± 6.20

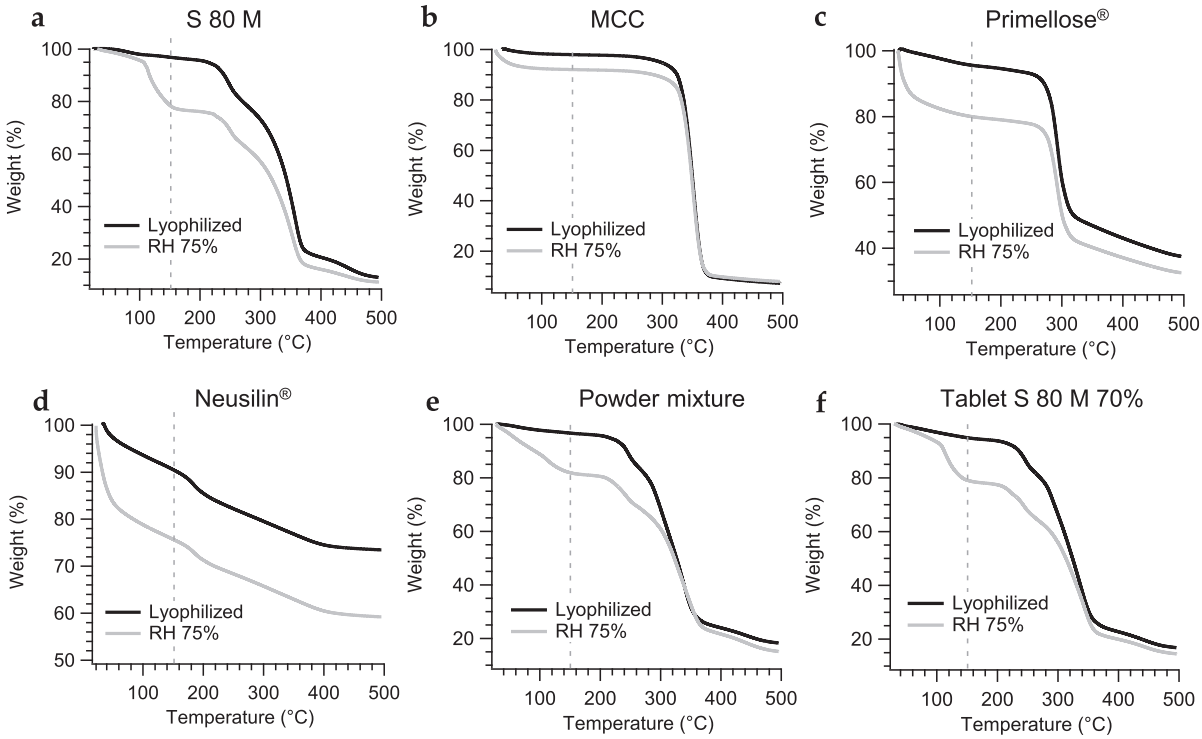

Fig. 1. TGA curves of the tablets' components (a-d), their mixture (e) and the tablet S 80 M 70% (f). The black curves indicate the freeze-dried samples, while the grey ones refer to the samples equilibrated at RH 75%. The dashed line at 150 °C indicates the point chosen for the estimate of the water amount gained upon equilibration at RH 75%.

Table 3
Water % (w/w) in the samples after equilibration at RH 75 %, obtained as difference between the weight loss % at 150 °C of samples equilibrated at RH 75% or freeze-dried. Mean ± S.D. (n = 3).

Sample	Water % (w/w)
S 80 M	19.3 ± 2.9
MCC	4.6 ± 1.2
Primellose®	17.4 ± 2.9
Neusilin®	14.1 ± 1.9
Powder mixture	17.0 ± 3.3
Tablet S 80 M 70 %	16.8 ± 0.9

Charman, 1997; Tso and Balint, 1986; Nayak et al., 2001; Tso et al., 1987).

The bioactivity of the extracted S 80 M was tested over a 24 h incubation time, fixing the total lipid concentration at 5 mM on cells for all the treatment conditions on naïve LX-2 immortalized hepatic stellate cells following our optimized *in vitro* model (Valentino et al., 2019).

No treatment interfered with LX-2 cell viability, thus excluding any possible toxicity of S 80 M (Fig. 4a), as expected from our previous studies (Valentino et al., 2019). S 80 M liposomes and extracts did not contribute to oxidative stress, as proven by the ROS level, which did not increase after treatment (Fig. 4b).

After establishing the effect of PPC on metabolic activity and toxicity, we quantified the changes in lipid droplet storage, evaluated variations in cellular membrane motional order, and followed the expression for the most important fibrosis marker genes as a function of the lipid treatments.

The Oil Red O (ORO) staining of neutral lipid droplets in LX-2 cells reveals the content of lipid droplets in the cell by fluorescence. ORO staining is among the gold standard methods to rapidly quantify the reversion of HSCs from an activated, profibrogenic status, depleted of lipid droplets, to a non-fibrogenic quiescent-like phenotype, characterized by distinct storage of lipid droplets (Seebacher et al., 2020).

As expected, LX-2 incubation with control conditions DMEM, DOPC, and PFC induced the formation of lipid droplets only to a negligible, non-significant amount (Fig. 4c and 4d); on the contrary, all the S 80 M treatments (Lipo, Tbl 70%, Tbl 70% + PFC) contributed to a significant increase ($p < 0.0001$) in the number of HSCs' lipid droplets, clearly visible as red spots in fluorescent images, with a ~ 36-fold increase in FRI compared to untreated LX-2 (DMEM) (57.1 FRI, 58.8 FRI and 59.7 FRI for Lipo, Tbl 70% and Tbl 70% + PFC treatments, respectively) in agreement with what previously been observed previously (Valentino et al., 2019). The differences between different S 80 M treatments were not significant.

These data clearly convey that both S 80 M extracts still retained significant bioactivity even after extensive technical processing. The findings are entirely in agreement with what has been observed previously (Valentino et al., 2019) and confirm a PPC-specific bioactivity in reverting of activated HSCs to a quiescent-like phenotype by restoration of lipid droplet content.

3.5. *mRNA transcription of fibrosis markers*

To further assess PPC lipid extracts' bioactivity we chose to analyse the mRNA transcription of some prominent markers of fibrosis, namely PLIN2, PDGFRB, ACTA2 coding for α-smooth muscle actin (α-SMA), COL1A1 for collagen type I, and SPARC, a membrane-associated protein, recently reported by our group (Zivko et al., 2022) to be associated with extracellular vesicles harvested and purified from activated LX-2. PLIN2 (perilipin 2) is a cytoplasmatic protein involved in lipid droplet formation, stabilization and lysis and its upregulation leads to a regulation of lipid droplets metabolism that are depleted in fibrotic pathological condition (Londos et al., 2005; Lee, 2010; Molenaar et al., 2017). Upregulation of PLIN2 has been demonstrated to be associated with a reduction of activation of HSCs and be connected with the reduction of

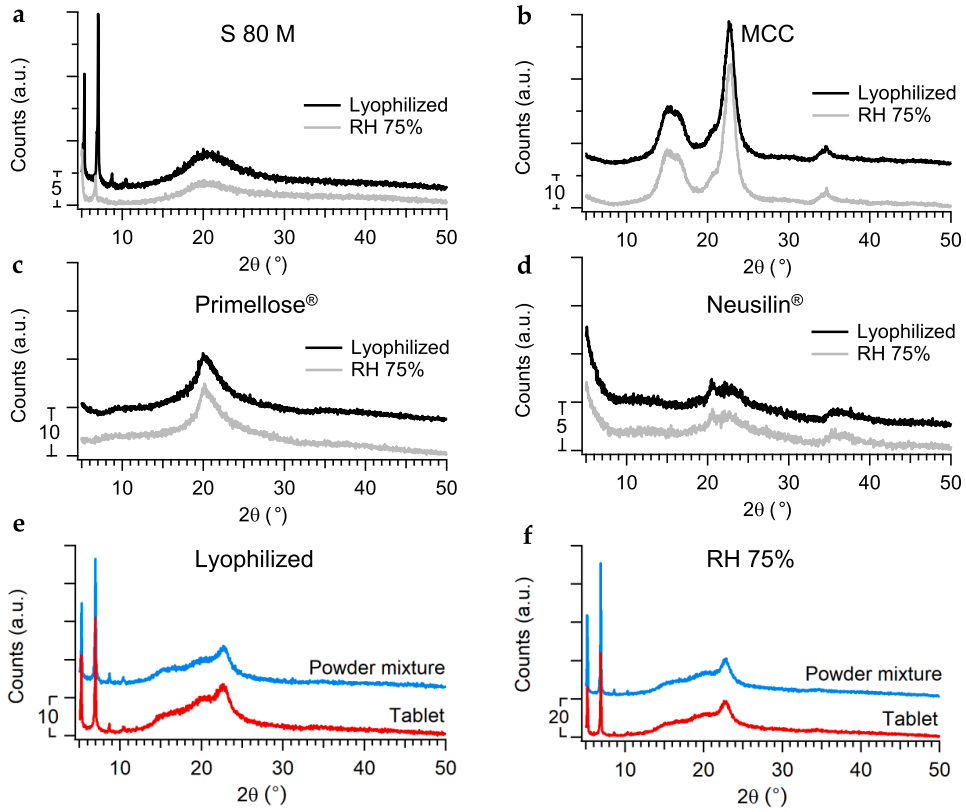

Fig. 2. XRPD diffractograms of (a) S 80 M, (b) MCC, (c) Primellose®, (d) Neusilin®. The black patterns refer to the freeze-dried samples, while the grey ones belong to the samples equilibrated at RH 75%. (e) freeze-dried tablet S 80 M 70% (red) and powder mixture before tableting (blue) samples. (f) tablet S 80 M 70% before (blue) and after (red) tableting equilibrated at RH 75%. All the diffractograms have been vertically offset for display purposes.

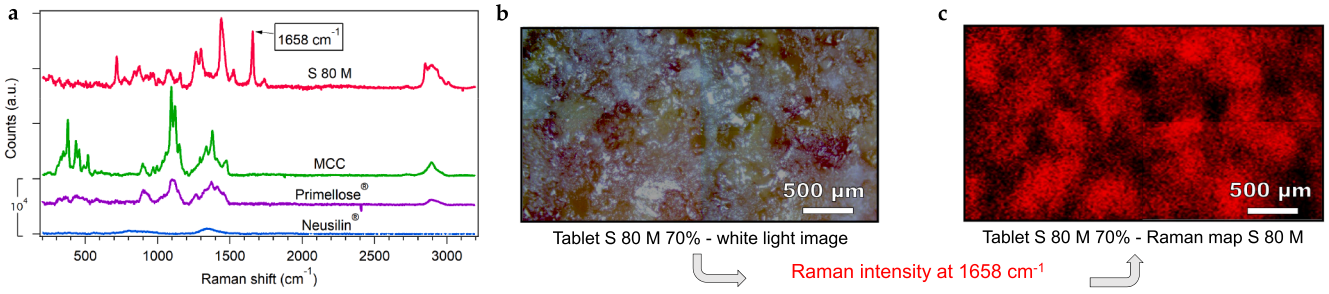

Fig. 3. (**a**) Raman spectra of the components present in the tablets. From the top to the bottom: S 80 M, MCC, Primellose® and Neusilin®. The spectra have been vertically offset for display purposes. (**b**) and (**c**) refer to the confocal Raman characterization of the Tablet S 80 M 70%. (**b**) White light image of the area under investigation. (**c**) Raman map showing the intensity at 1658 cm^{-1}, indicating the distribution of S 80 M within the tablet.

some prominent fibrotic markers (such as collagen type I, α-SMA, matrix metalloprotease 2 – MMP-2) *via* intracellular mechanisms that remain undefined (Lee, 2010).

Platelet-derived growth factor receptor-β (PDGFR-β) is a tyrosine kinase transmembrane protein. This specific isoform mediates the activation and increase in profibrogenic transdifferentiation of HSCs into myofibroblasts during hepatic fibrosis (Kocabayoglu, 2015; Kikuchi, 2020; Lambrecht, 2019). A rapid increase in the expression of PDGFR-β has been shown to sustain pathological progression by modulating multiple intracellular pathways (Kocabayoglu, 2015; Kikuchi, 2020; Lambrecht, 2019). Its reduced expression correlates with decreased HSC activation and ameliorated fibrosis progression (Kocabayoglu, 2015) by reverting HSCs back to a quiescent-like phenotype.

Cells treated with S 80 M extracts significantly maximized PLIN2 mRNA expression of 2.8-fold, 2.6-fold and 3.0-fold for Lipo, Tbl 70% and Tbl 70% + PFC, respectively. As PLIN2 expression is connected with lipid droplet metabolism, the observed upregulation of this gene confirms the increase in fluorescence quantified with the ORO staining (Fig. 4b).

In the case of PDGFRB mRNA expression, cells treated with S 80 M showed a decrease of ~ 45%, ~49% and ~ 42% (Lipo, Tbl 70 % and Tbl 70 % + PFC, respectively), which means lipid extracts managed to revert cells to a quiescent-like phenotype by reducing the mRNA transcription. PDGFR-β activation leads to enhanced signalling along the Fas-MAPK pathway, and further to the PI3K-AKT/PKB pathway with involvement of PKC family members (Kocabayoglu, 2015; Donovan et al., 2013). Particularly, the activation of ERK2 and ERK5 (part of MAPK family) axis has been associated with increased cell migration, proliferation, transdifferentiation and inflammation (Rovida et al., 2008; Jeng et al., 2020). Expression of soluble PDGFR-β in blood has been studied to be

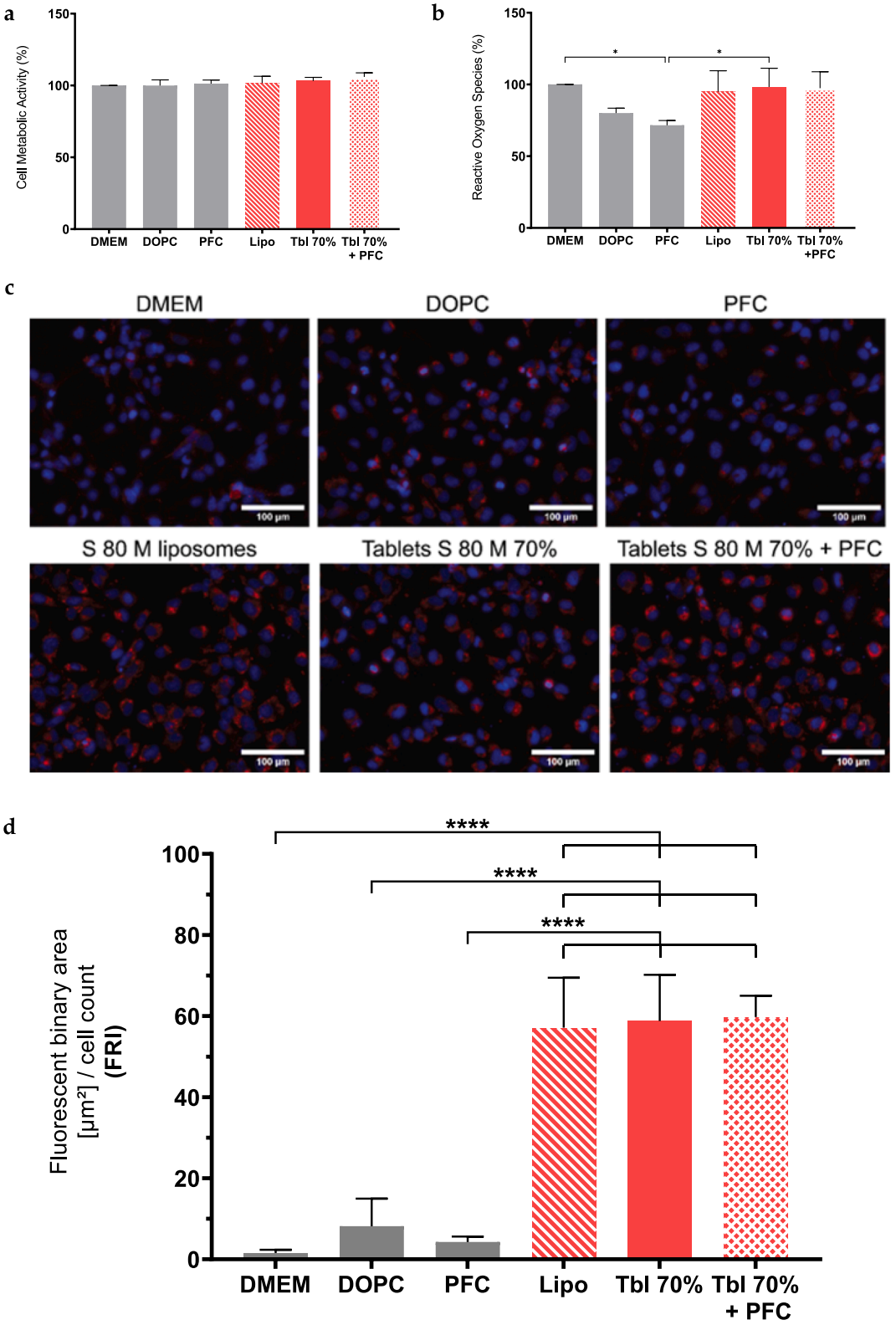

Fig. 4. (**a**) LX-2 cell viability (%) using CCK-8 assay. (**b**) LX-2 ROS production. (**c-d**) ORO staining of LX-2 cells treated with various phospholipid treatments: DMEM experimental medium (untreated); DOPC: inactive phospholipid used as negative control; PFC: protein-free chylomicron-like emulsions without S 80 M; Lipo: S 80 M liposomes; Tbl 70%: S 80 M tablet extract in buffer; Tbl 70% + PFC: tablet extract reconstituted as PFC-like emulsions. (**c**) Representative fluorescence images of LX-2 cells in which lipid droplets can be visualized as red spots and the nuclei are counterstained with blue DAPI. (**d**) Quantification of the ORO fluorescence normalized to the number of LX-2 cells in the DAPI field (FRI). Cell number per image was in range ~ 50–160 cells. Mean ± S.D. (n = 3). p-values (**** $p < 0.0001$, * $p < 0.05$) from ordinary one-way ANOVA with *post-hoc* Tukey's multiple comparison analysis.

used as a valid parameter in clinical prognosis of the fibrosis state of patients by Lambrecht *et al.* (Lambrecht, 2019). To confirm the validity of system, expression levels of PDGFRB were assessed and were found to be notably lower in healthy/quiescent HSCs (primary human and mouse HSCs). PDGFR-β antagonism is considered a desirable target to treat hepatic fibrosis (Kocabayoglu, 2015; Kim, 2012; Reichenbach, 2012; Borkham-Kamphorst, 2008). It has beendemonstrated that imatinib mesylate (a tyrosine kinase inhibitor, Gleevec®), a potent inhibitor of PDGFR-β, was able to inhibit HSC activation and sequentially reduce early fibrosis, but the progression of the pathology was not prevented (Neef, 2006).

SPARC is a matricellular glycoprotein whose main function is exerted by mediating the interactions between cells and their extracellular matrix with respective tissue remodeling including those undergoing wound repair or morphogenesis (Barker, 2005; Trombetta-Esilva and Bradshaw, 2012; Camino, 2008). Its upregulation in hepatic fibrosis pathways has been previously demonstrated in LX-2 cells and in human biopsies (Mazzolini, 2018; Onorato et al., 2021; Wang et al., 2020), suggesting that downregulating SPARC could be part of a therapeutic approach to revert the pathology. SPARC is associated with the extracellular portion of the plasma membrane and we recently reported that EVs from LX-2 cells treated with S80, a PPC-rich lipid analogue to S 80 M, have a remarkably lower level of SPARC associated with their membrane measured via fluorescence nanoparticle-tracking analysis (Zivko et al., 2022; Zivko et al., 2023).

In our experimental design, no statistically significant change in mRNA transcription of ACTA2, COL1A1, and SPARC markers could be observed, although it could be observed that all the S 80 M treatments contributed to a slight decrease of the relative values with respect to naïve cells (**Figure S5**).

Since liver fibrosis employs more than 150 differently expressed markers in HSCs, (He et al., 2020) looking at only a few genetic markers selected *ad hoc* and assays could give us a rapid insight into the bioactivity of PPCs, however, these results alone cannot preclude that other biological effects of S 80 M treatments could occur. Nevertheless, the observed decrease in PDFGRB and increase in PLIN2 mRNA transcription levels and the lipid droplets recovery in ORO staining upon incubation with S 80 M suggest that PPC contributes to restoring a quiescent-like status, as observed also by other groups (Lee, 2010; O'Mahony, 2015), and that handling the PPCs to manufacture tablets does not interfere with their biological activity. Further extensive transcriptomics and proteomics studies are planned to shed light on the pathways involved and to understand whether a proper de-activation of HSCs takes place.

3.6. Motional order of the cell membrane in adherent LX-2 cells

The dynamic properties of membrane lipids in relation to the treatments were assessed by calculating the anisotropy of DPH and TMA-DPH from fluorescence polarization experiments. DPH is a probe known to arrange itself in the inner core of the bilayer, while TMA-DPH is at the interface region owing to its amphiphilic nature (do Canto et al., 2016). Therefore, DPH could be employed to estimate the motional order of the hydrophobic membrane region, while TMA-DPH senses changes in motional order in the region at the interface with the extracellular space. Independently of the probe used, a decrease of anisotropy corresponds to an increased motional order of the cell membrane and thus to a higher membrane fluidity (Fig. 5).

All S 80 M treatments significantly increased the motional order of the inner membrane layer, shown in Fig. 6a, compared to DMEM. Lipo, Tbl 70% and Tbl 70% + PFC caused a decrease in measured DPH anisotropy from 0.224 (untreated) to 0.208 (-7.1%), 0.204 (- 8.9%) and 0.199 (-11.5%), respectively.

At the interfacial region (Fig. 6b) Tbl 70% and Tbl 70% + PFC significantly increased the motional order of the membrane with respect to untreated DMEM. Measured TMA-DPH anisotropy was decreased from 0.255 to 0.248 (-2.8%, Lipo), 0.234 (-8.1 %, Tbl 70%) and 0.238 (-6.5 %, Tbl 70% + PFC). Overall, PPC treatments of LX-2 cells affected the motional order of the cell membrane more at the interfacial level than in the hydrophobic core.

The increase in liver tissue stiffness observed in fibrosis and caused by HSCs myofibroblastic transdifferentiation and extracellular matrix (ECM) accumulation (Saneyasu et al., 2016; Sakata et al., 2004; Chiabotto et al., 2022) is related to a change in the cell membrane motional order. Our measurements of fluorescent anisotropy on living adherent cells provided us with a one-of-a-kind insight into the effects of treatments with PPC tablet extract on cell membrane fluidity. The SPARC mRNA transcription results (Figure S5c), though, suggest that the beneficial action of S 80 M doesn't interfere with the mRNA expression itself but rather with the mesoscale properties of the cell membrane – namely its stiffness at the interface (Fig. 6b) – the region where SPARC docks to exert its ECM orchestrating function.

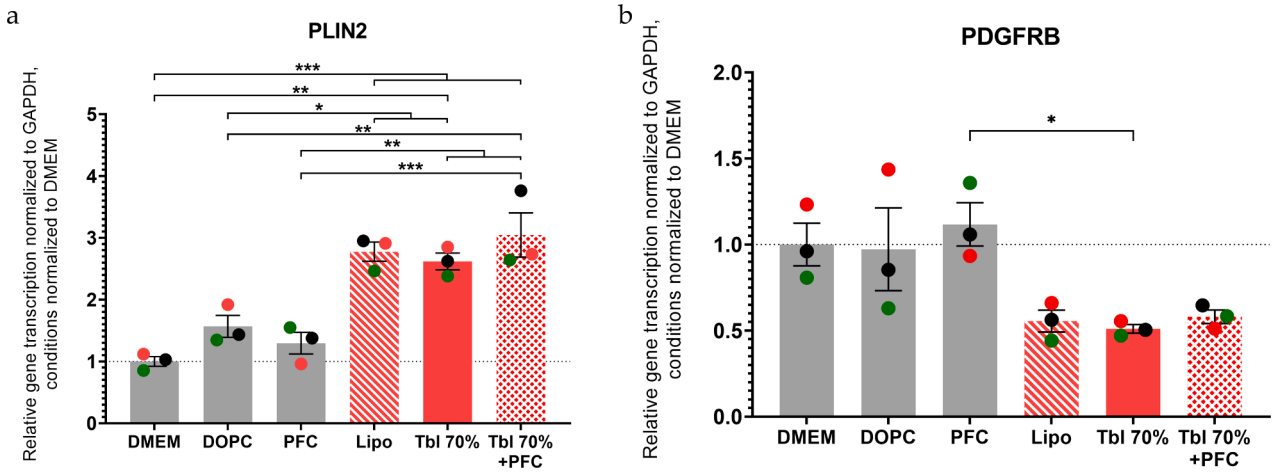

Fig. 5. Relative mRNA transcription in LX-2 cells of two fibrosis markers (a) PLIN2 and (b) PDGFRB, normalized to GAPDH mRNA transcription and normalized to the DMEM condition after different phospholipid treatments: DMEM experimental medium (untreated); DOPC: inactive phospholipid used as negative control; PFC: protein-free chylomicron-like emulsions without S 80 M; Lipo: S 80 M liposomes; Tbl 70%: S 80 M tablet extract in buffer; Tbl 70% + PFC: tablet extract reconstituted as PFC-like emulsions. Mean ± S.E.M. (n = 3). p-values (*** $p < 0.001$, ** $p < 0.01$, * $p < 0.05$) from ordinary one-way ANOVA with *post hoc* Tukey's multiple comparison analysis.

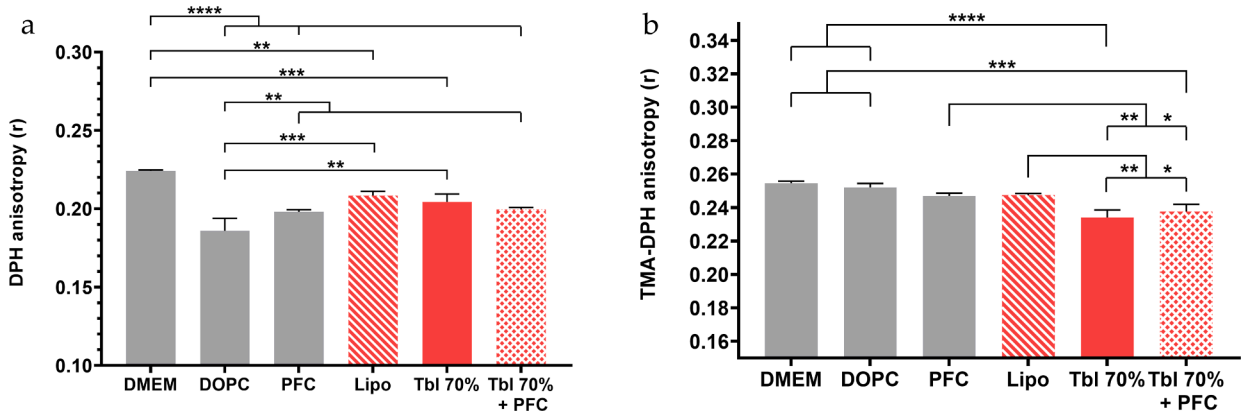

Fig. 6. PPC treatment effect on the motional order of LX-2 cell membrane by means of anisotropy of (a) DPH (inner membrane) and (b) TMA-DPH (interfacial membrane) as a function of different phospholipid treatments: DMEM experimental medium (untreated); DOPC: inactive phospholipid used as negative control; PFC: protein-free chylomicron-like emulsions without S 80 M; Lipo: S 80 M liposomes; Tbl 70%: S 80 M tablet extract in buffer; Tbl 70% + PFC: tablet extract reconstituted as PFC-like emulsions. Mean ± S.D. (n = 3). p-values (**** $p < 0.0001$, *** $p < 0.001$, ** $p < 0.01$, * $p < 0.05$) from ordinary one-way ANOVA with *post hoc* Tukey's multiple comparison analysis.

3.7. Modulation of cirrhotic PRHSCs phenotype indicating antifibrogenic effects: Our proof of principle

The biological tests carried out to establish the possible hepatoprotective function of PPC tablets were all conducted on LX-2 cells, a model of activated human immortalized HSCs. In the attempt to move toward preclinical studies, we decided to validate our findings in primary rat HSCs from cirrhotic rats (Fernandez-Iglesias et al., 2019).

Although liver fibrosis does not always proceed to end-stage liver disease, we hypothesized that demonstrating that our formulations could de-activate highly fibrogenic HSCs could be a compelling first piece of data for upcoming *in vivo* studies.

We screened the treatments on cirrhotic PRHSCs adopting the same experimental design used in LX-2 cells. Briefly, S 80 M extracted from tablets was reconstituted and tested on cells over a 24 h incubation time, fixing the total lipid concentration at 5 mM. We observed the same trends in PRHSCs as in LX-2 (Fig. 4). Specifically, none of the treatments interfered with cell viability, excluding thus any possible toxicity of S 80 M (Fig. 7a). S 80 M liposomes and extracts did not contribute to oxidative stress, as proven by the ROS level which did not increase after treatment (Fig. 7b).

Cirrhotic PRHSCs treated with Lipo showed a significant increase in the number of lipid droplets, while Tbl 70% and Tbl 70% + PFC followed the same trend and were of similar magnitude, but did not reach statistical significance. Lipid treatments induced a ~ 14-fold increase in FRI in comparison with IMDM (51.0 FRI, 46.3 FRI and 44.31 FRI for Lipo, Tbl 70%, and Tbl 70% + PFC treatments, respectively; Fig. 7ab). S 80 M Lipo had a slightly higher impact on lipid droplet content, but the difference compared to other S 80 M treatments was not significant.

Rat quiescent HSCs physiologically express lipid droplets in the cytoplasm as a storage for physiological retinoic esters similar to what was observed in HSCs from other sources (human, mouse). Lipid droplets disrupt once HSCs transdifferentiate in case of injury to the liver, a phenomenon that ultimately may lead to a change in the cellular architecture and to ECM accumulation (Blaner, 2009). Recovery of lipid droplets in cirrhotic PRHSCs is analogous to that observed in directly treated activated LX-2 cells. This suggests that S 80 M had a similar effect on lipid metabolism of PRHSCs, even if general pathological cell state was more advanced, since usually rat HSCs express similar metabolic pathways as human ones.

To investigate whether PPC treatment would exert the same fluidising effect observed in LX-2 cells, the motional order of the membrane of primary cells was quantified (Fig. 8).

Tbl 70% and Tbl 70% + PFC significantly increased the motional order of the inner membrane layer compared to IMDM (Fig. 8a). Lipo, Tbl 70%, and Tbl 70% + PFC caused a decrease in measured DPH anisotropy from 0.269 (untreated) to 0.211 (-21.5% relative to untreated), 0.166 (-38.3% relative to untreated) and 0.166 (-38.4% relative to untreated), respectively. The other S 80 M treatments were not significantly different. Lipo appears to have only a moderate effect on inner membrane motility. The reduction of stiffness of PRHSC membrane seemed to be induced in its deep hydrophobic core, as at the interfacial region (Fig. 8b), S 80 M extracts did not induce any significant variation.

PFC had the strongest effect on decreasing both DPH and TMA-DPH anisotropy, allowing a higher degree of cellular membrane motility, although this effect was not additive to the tablet extract treatment. In this latter case, indeed, the anisotropy values remained unchanged when the extracted lipids were reconstituted in PFC emulsions (Fig. 8ab).

4. Conclusion

The PPC-rich soy phospholipid S 80 M has physical properties suitable to generate a lipid powder mixture via dry granulation. The good flowability of the lipid powder was maintained even with 70% of bioactive lipids and the subsequent compression of the lipid mixture into tablets led to a dosage form complying with the major pharmacopoeial requirements. PPCs extracted from tablets were tested with a dynamic fibrogenic cell model of human immortalized HSCs and rat cirrhotic PRHSCs and in all cases the PPC treatments reverted the fibrogenic phenotype of HSCs, resulting in increased lipid storage, and in an increase of the membrane fluidity correlated with improvement of the fibrotic state of HSCs. mRNA transcription data showing an increase in PLIN2 and a decrease in PDGFRB levels in LX-2 cells supports our hypothesis of an antifibrotic effect of S 80 M treatments. Mimicking the uptake of PPCs in remnant chylomicrons using a chylomicron-like emulsion was comparable to pure PPCs in both LX-2 and PRHSCs in all experimental conditions.

We believe that our findings shed new light on understanding that sensitive, complex, technically challenging yet bioactive phospholipids, such as the natural PPC-rich S 80 M, can be formulated into tablets, which are a more patient-centric, simple-to-manufacture pharmaceutical dosage form. PPCs retained their physicochemical and bioactive properties, as demonstrated by our combination of technological characterization and biological assays performed on two different *in vitro* models of liver fibrosis and cirrhosis. The bioavailability and pharmacological action of these lipid-based products will be clarified by upcoming *in vivo* studies, which will provide more information on the

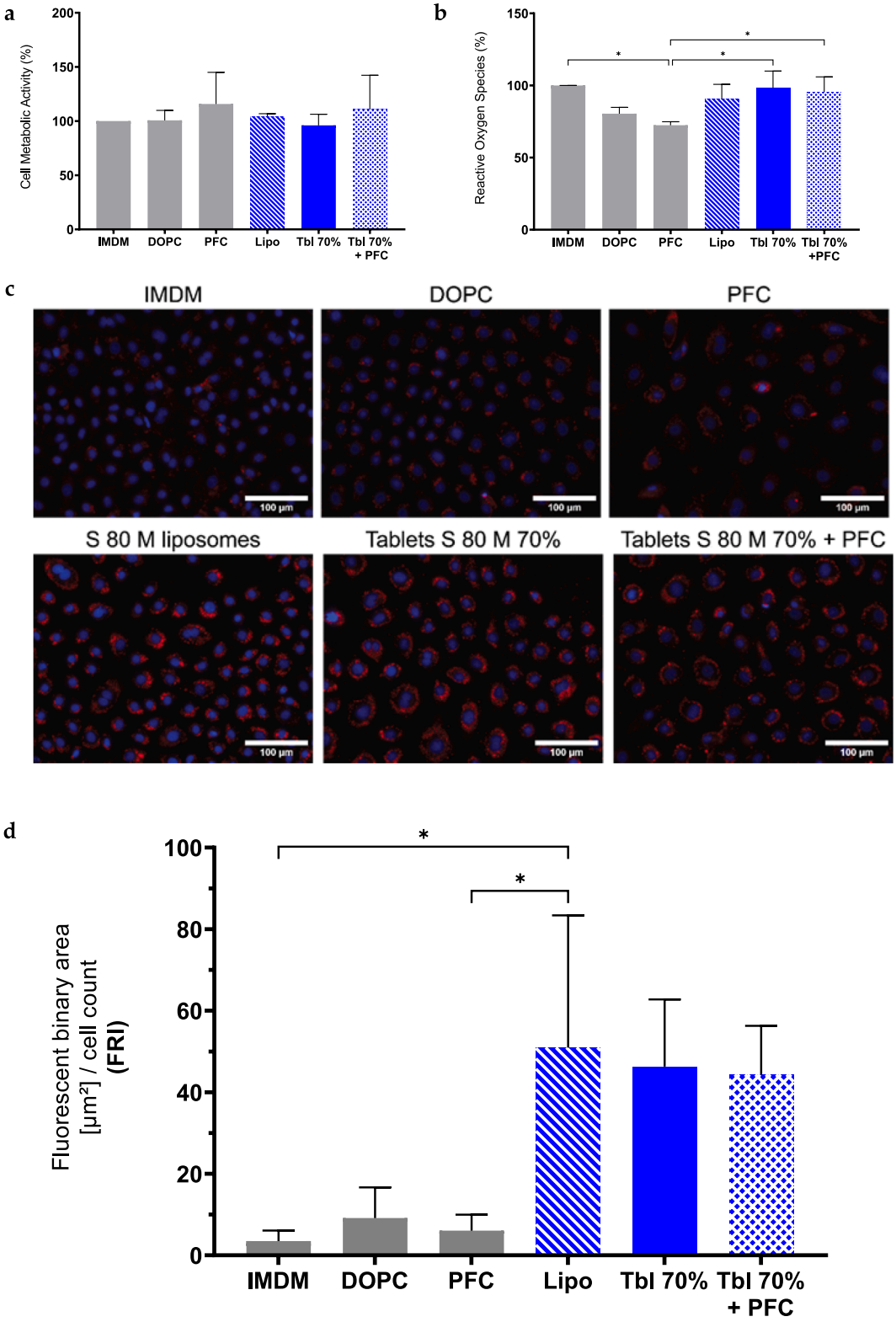

Fig. 7. (a) PRHSCs cell viability (%) using CCK-8 assay. (b) PRHSCs ROS production. (c-d) ORO staining of cirrhotic PRHSCs treated with various phospholipid treatments: IMDM: experimental medium; DOPC: inactive phospholipid used as negative control; PFC: protein-free chylomicron-like emulsions without S 80 M; Lipo: S 80 M liposomes; Tbl 70%: S 80 M tablet extract in buffer; Tbl 70% + PFC: tablet extract reconstituted as PFC-like emulsions. (**c**) Representative images of PRHSCs. (d) Quantification of the ORO fluorescence normalized to the number of PRHSCs in the DAPI field (FRI). Cell number per image was in range ~ 5–150 cells. Mean ± S.D. (n = 3). p-values (* $p < 0.05$) from ordinary one-way ANOVA with *post hoc* Tukey's multiple comparison analysis.

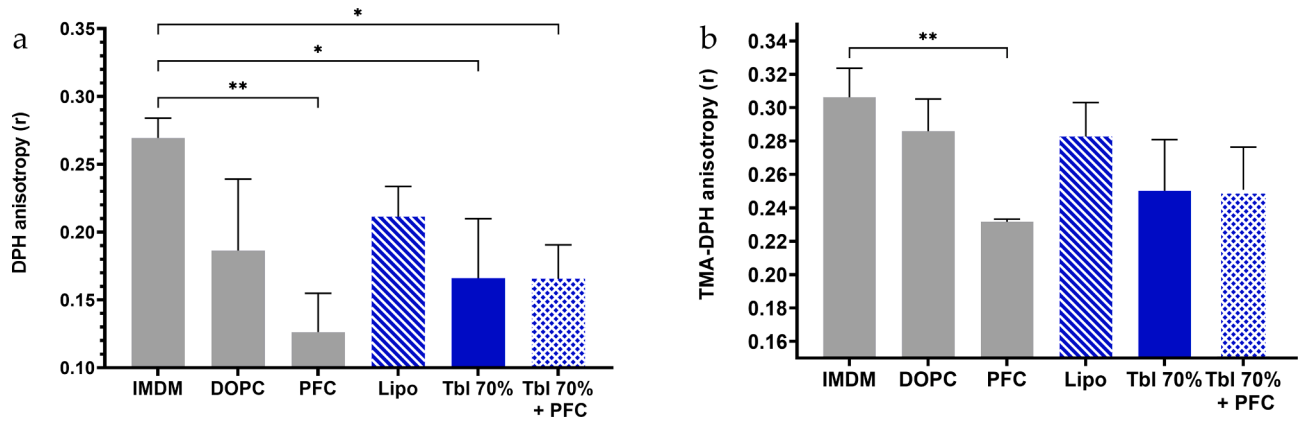

Fig. 8. PPC treatment effect on the motional order of PRHSC cell membrane by means of anisotropy of (a) DPH (inner membrane) and (b) TMA-DPH (interfacial membrane) as a function of different phospholipid treatments: IMDM experimental medium (untreated); DOPC: inactive phospholipid used as negative control; PFC: protein-free chylomicron-like emulsions without S 80 M; Lipo: S 80 M liposomes; Tbl 70%: S 80 M tablet extract in buffer; Tbl 70% + PFC: tablet extract reconstituted as PFC-like emulsions. Mean ± S.D. (n = 3). p-values (** $p < 0.01$, * $p < 0.05$) from ordinary one-way ANOVA with *post hoc* Tukey's multiple comparison analysis.

potential of PPC-tablets for the pharmacological management of chronic liver diseases.

CRediT authorship contribution statement

Ivo Skorupdevised and performed all the tableting and *in vitro* and *ex vivo* experiments, developed methodology, analyzed the data, co-wrote the original draft; **Gina Valentino** conceived the original project, devised and performed pilot experiments, developed methodology, co-wrote the original draft; **Simone Aleandri** devised experiments and methodology, contributed to data curation, co-wrote the original draft; **Rita Gelli** performed physicochemical analysis (TGA, XRPD, Raman), co-wrote the original draft; **Aymar Abel Ganguin** devised qPCR methodology and helped performing and analysing qPCR experiments; **Eric Felli** devised methodology with rat primary cells, consulted on data analysis and edited the manuscript; **Rosanne Angela Marxer** devised and validated methodology; **Sonia Emilia Selican** devised methodology with rat primary cells; **Sarah Teworte** devised and validated methodology (HPLC-CAD) and edited the manuscript; **Ana Lucić** devised and validated methodology (HPLC-CAD); **Jordi Gracia-Sancho** and **Annalisa Berzigotti** provided resources and funding, revised and edited the manuscript; **Francesca Ridi** supervised Rita Gelli's research work, revised and edited the manuscript; **Paola Luciani** conceived and supervised the original project, provided funding, administered the project, reviewed and edited the manuscript.

Declaration of Competing Interest

The authors declare the following financial interests/personal relationships which may be considered as potential competing interests: No private study sponsors had any involvement in the study design, data collection, or interpretation of data presented in this manuscript. Paola Luciani. has consulted and received research grants from Lipoid GmbH, Sanofi-Aventis Deutschland, and DSM Nutritional Products Ltd. Annalisa Berzigotti is consultant for Boehringer-Ingelheim. Jordi Gracia-Sancho has received research funding from Gilead Sciences, Inventiva, Conatus, Surrozen, GAT Tx, BrudyLab and Quinton International, and acted as consultant for Ambys, Novo Seeds, Kintsugi Tx, BrudyLab and Terrafirma. All the other co-authors declare no competing interests.

Data availability

Data will be made available on request.

Acknowledgements

We would like to thank Cong Wang and Yeliduosi Nulan from Hepatology Research Group at DBMR, University of Bern for support with PRHSCs. Special thanks go to Dr. Sofia Nasif, Nicole Kleinschmidt and Prof. Dr. Oliver Mühlemann from DCBP, University of Bern for providing support with qPCR experiments. The graphical abstract has been created using Biorender.com.

Lipoid GmbH is kindly acknowledged for providing Soluthin® S 80 M; IMCD Switzerland AG for providing Neusilin® US2; Evonik Industries AG for providing Eudragit® L100-55; DFE Pharma GmbH for providing Primellose®. Annalisa Berzigotti acknowledges the support from Swiss National Science Foundation (320030_189252). Jordi Gracia-Sancho is supported by the Instituto de Salud Carlos III (FIS PI20/00220 and DTS22/00010, co-funded by the European Union), the CIBEREHD, the Swiss National Science Foundation (320030_189252), the Novartis Foundation for Medical-Biological Research and the Foundation Suisse Contre le Cancer du Foie. CIBEREHD is funded by the Instituto de Salud Carlos III.

Appendix A. Supplementary data

Supplementary data to this article can be found online at https://doi.org/10.1016/j.ijpharm.2023.123473.

References

Azad, M., Moreno, J., Dave, R., 2018. Stable and fast-dissolving amorphous drug composites preparation via impregnation of Neusilin® UFL2. J. Pharm. Sci. 107, 170–182. https://doi.org/10.1016/j.xphs.2017.10.007.

Barker, T.H., et al., 2005. SPARC regulates extracellular matrix organization through its modulation of integrin-linked kinase activity. J. Biol. Chem. 280, 36483–36493. https://doi.org/10.1074/jbc.M504663200.

Blaner, W.S., et al., 2009. Hepatic stellate cell lipid droplets: A specialized lipid droplet for retinoid storage. Biochim. Biophys. Acta 1791, 467–473. https://doi.org/10.1016/j.bbalip.2008.11.001.

Bligh, E.G., Dyer, W.J., 1959. A rapid method of total lipid extraction and purification. Can. J. Biochem. Physiol. 37, 911–917. https://doi.org/10.1139/o59-099.

Borkham-Kamphorst, E., et al., 2008. Platelet-derived growth factor isoform expression in carbon tetrachloride-induced chronic liver injury. Lab. Invest. 88, 1090–1100. https://doi.org/10.1038/labinvest.2008.71.

Camino, A.M., et al., 2008. Adenovirus-mediated inhibition of SPARC attenuates liver fibrosis in rats. J. Gene Med. 10, 993–1004. https://doi.org/10.1002/jgm.1228.

Chakraborty, S., Shukla, D., Vuddanda, P.R., Mishra, B., Singh, S., 2010. Utilization of adsorption technique in the development of oral delivery system of lipid based nanoparticles. Colloids Surf. B Biointerfaces 81, 563–569. https://doi.org/10.1016/j.colsurfb.2010.07.058.

Chapman, D., Collin, D.T., 1965. Differential thermal analysis of phospholipids. Nature 206, 189. https://doi.org/10.1038/206189a0.

Chiabotto, G., Ceccotti, E., Bruno, S., 2022. Narrative review of in vitro experimental models of hepatic fibrogenesis. Dig. Med. Res. 5, 33. https://doi.org/10.21037/dmr-21-102.
do Canto, A., et al., 2016. Diphenylhexatriene membrane probes DPH and TMA-DPH: A comparative molecular dynamics simulation study. Biochim. Biophys. Acta 1858, 2647–2661. https://doi.org/10.1016/j.bbamem.2016.07.013.
Donovan, J., Abraham, D., Norman, J., 2013. Platelet-derived growth factor signaling in mesenchymal cells. Front Biosci (landmark Ed) 18, 106–119. https://doi.org/10.2741/4090.
Fernandez-Iglesias, A., Ortega-Ribera, M., Guixe-Muntet, S., Gracia-Sancho, J., 2019. 4 in 1: Antibody-free protocol for isolating the main hepatic cells from healthy and cirrhotic single rat livers. J. Cell Mol. Med. 23, 877–886. https://doi.org/10.1111/jcmm.13988.
Grune, L., Bunjes, H., 2020. Suitability of phosphatidylcholine-based formulations for liquid filling in hard capsules. Eur. J. Pharm. Sci. 153, 105470. https://doi.org/10.1016/j.ejps.2020.105470.
Gundermann, K.J., 1993. The "Essential" Phospholipids as a Membrane Therapeutic. Polish Section of European Society of Biochemical Pharmacology, Szczecin.
Gundermann, K.J., Gundermann, S., Drozdzik, M., Mohan Prasad, V.G., 2016. Essential phospholipids in fatty liver: A scientific update. Clin. Exp. Gastroenterol. 9, 105–117. https://doi.org/10.2147/CEG.S96362.
Hauss, D.J., 2007. Oral Lipid-Based Formulations: Enhancing the Bioavailability of Poorly Water-Soluble Drugs, 1 ed. CRC Press.
He, L., Yuan, H., Liang, J., Hong, J., Qu, C., 2020. Expression of hepatic stellate cell activation-related genes in HBV-, HCV-, and nonalcoholic fatty liver disease-associated fibrosis. PLoS One 15, e0233702.
Hentzschel, C.M., Sakmann, A., Leopold, C.S., 2011. Suitability of various excipients as carrier and coating materials for liquisolid compacts. Drug Dev. Ind. Pharm. 37, 1200–1207. https://doi.org/10.3109/03639045.2011.564184.
Jeng, K.S., Lu, S.J., Wang, C.H., Chang, C.F., 2020. Liver fibrosis and inflammation under the control of ERK2. Int. J. Mol. Sci. 21, 3796. https://doi.org/10.3390/ijms21113796.
Kapoor, D. et al. in *Drug Delivery Systems* (ed Rakesh K. Tekade) 665-719, Academic Press, 2020.
Kikuchi, A., et al., 2020. Hepatic stellate cell-specific platelet-derived growth factor receptor-alpha loss reduces fibrosis and promotes repair after hepatocellular injury. Am. J. Pathol. 190, 2080–2094. https://doi.org/10.1016/j.ajpath.2020.06.006.
Kim, Y., et al., 2012. Anti-fibrotic activity and enhanced interleukin-6 production by hepatic stellate cells in response to imatinib mesylate. Liver Int. 32, 1008–1017. https://doi.org/10.1111/j.1478-3231.2012.02806.x.
Kocabayoglu, P., et al., 2015. Beta-PDGF receptor expressed by hepatic stellate cells regulates fibrosis in murine liver injury, but not carcinogenesis. J. Hepatol. 63, 141–147. https://doi.org/10.1016/j.jhep.2015.01.036.
Koch, N., Jennotte, O., Toussaint, C., Lechanteur, A., Evrard, B., 2023. Production challenges of tablets containing lipid excipients: Case study using cannabidiol as drug model. Int. J. Pharm. 633, 122639. https://doi.org/10.1016/j.ijpharm.2023.122639.
Kochan, K., et al., 2016. IR and raman imaging of murine brains from control and ApoE/LDLR(-/-) mice with advanced atherosclerosis. Analyst 141, 5329–5338. https://doi.org/10.1039/c6an00107f.
Kolbina, M., Bodmeier, R., Korber, M., 2017. Saturated phosphatidylcholine as matrix former for oral extended release dosage forms. Eur. J. Pharm. Sci. 108, 86–92. https://doi.org/10.1016/j.ejps.2017.07.017.
Kolbina, M., Schulte, A., van Hoogevest, P., Korber, M., Bodmeier, R., 2019. Evaluation of hydrogenated soybean phosphatidylcholine matrices prepared by hot melt extrusion for oral controlled delivery of water-soluble drugs. AAPS PharmSciTech 20, 159. https://doi.org/10.1208/s12249-019-1366-3.
Kuentz, M., 2012. Lipid-based formulations for oral delivery of lipophilic drugs. Drug Discov. Today Technol. 9, e71–e174. https://doi.org/10.1016/j.ddtec.2012.03.002.
Lambrecht, J., et al., 2019. A PDGFRbeta-based score predicts significant liver fibrosis in patients with chronic alcohol abuse. NAFLD and Viral Liver Disease. *Ebiomedicine* 43, 501–512. https://doi.org/10.1016/j.ebiom.2019.04.036.
Lee, T.F., et al., 2010. Downregulation of hepatic stellate cell activation by retinol and palmitate mediated by adipose differentiation-related protein (ADRP). J. Cell. Physiol. 223, 648–657. https://doi.org/10.1002/jcp.22063.
Livak, K.J., Schmittgen, T.D., 2001. Analysis of relative gene expression data using real-time quantitative PCR and the 2(-Delta Delta C(T)) method. Methods 25, 402–408. https://doi.org/10.1006/meth.2001.1262.
Londos, C., Sztalryd, C., Tansey, J.T., Kimmel, A.R., 2005. Role of PAT proteins in lipid metabolism. Biochimie 87, 45–49. https://doi.org/10.1016/j.biochi.2004.12.010.
Maev, I.V., et al., 2019. Real-world comorbidities and treatment patterns among patients with non-alcoholic fatty liver disease receiving phosphatidylcholine as adjunctive therapy in Russia. BMJ Open Gastroenterol. 6, e000307. https://doi.org/10.1136/bmjgast-2019-000307.
Mazzolini, G., et al., 2018. SPARC expression is associated with hepatic injury in rodents and humans with non-alcoholic fatty liver disease. Sci. Rep. 8, 725. https://doi.org/10.1038/s41598-017-18981-9.
Molenaar, M.R., Vaandrager, A.B., Helms, J.B., 2017. Some lipid droplets are more equal than others: Different metabolic lipid droplet pools in hepatic stellate cells, 1178635317747281 Lipid Insights 10. https://doi.org/10.1177/1178635317747281.
Mortimer, B.C., et al., 1995. Features of cholesterol structure that regulate the clearance of chylomicron-like lipid emulsions. J. Lipid Res. 36, 2038–2053. https://doi.org/10.1016/S0022-2275(20)41121-6.
Nayak, N., Harrison, E.H., Hussain, M.M., 2001. Retinyl ester secretion by intestinal cells: a specific and regulated process dependent on assembly and secretion of chylomicrons. J. Lipid Res. 42, 272–280. https://doi.org/10.1016/S0022-2275(20)31689-8.
Neef, M., et al., 2006. Oral imatinib treatment reduces early fibrogenesis but does not prevent progression in the long term. J. Hepatol. 44, 167–175. https://doi.org/10.1016/j.jhep.2005.06.015.
O'Mahony, F., et al., 2015. Liver X receptors balance lipid stores in hepatic stellate cells through Rab18, a retinoid responsive lipid droplet protein. Hepatology 62, 615–626. https://doi.org/10.1002/hep.27645.
Onorato, A.M., et al., 2021. SPARC inhibition accelerates NAFLD-associated hepatocellular carcinoma development by dysregulating hepatic lipid metabolism. Liver Int 41, 1677–1693. https://doi.org/10.1111/liv.14857.
Pence, I., Mahadevan-Jansen, A., 2016. Clinical instrumentation and applications of raman spectroscopy. Chem. Soc. Rev. 45, 1958–1979. https://doi.org/10.1039/c5cs00581g.
Ph. Eur. 11.0, 0478 (01/2023). https://www.edqm.eu/documents/52006/436234/Webinar+Ph.Eur+General+notices+7+April+2022.pdf/c150ff27-eda5-d12c-0bc2-2a7cc8dbebf2?t=1652704721572.
Porter, C.J.H., Charman, W.N., 1997. Uptake of drugs into the intestinal lymphatics after oral administration. Adv. Drug Del. Rev. 25, 71–89. https://doi.org/10.1016/S0169-409x(96)00492-9.
Rahnfeld, L., Thamm, J., Steiniger, F., van Hoogevest, P., Luciani, P., 2018. Study on the in situ aggregation of liposomes with negatively charged phospholipids for use as injectable depot formulation. Colloids Surf. B Biointerfaces 168, 10–17. https://doi.org/10.1016/j.colsurfb.2018.02.023.
Reichenbach, V., et al., 2012. Adenoviral dominant-negative soluble PDGFRbeta improves hepatic collagen, systemic hemodynamics, and portal pressure in fibrotic rats. J. Hepatol. 57, 967–973. https://doi.org/10.1016/j.jhep.2012.07.012.
Rovida, E., Navari, N., Caligiuri, A., Dello Sbarba, P., Marra, F., 2008. ERK5 differentially regulates PDGF-induced proliferation and migration of hepatic stellate cells. J. Hepatol. 48, 107–115. https://doi.org/10.1016/j.jhep.2007.08.010.
Sakata, R., Ueno, T., Nakamura, T., Ueno, H., Sata, M., 2004. Mechanical stretch induces TGF-beta synthesis in hepatic stellate cells. Eur. J. Clin. Invest. 34, 129–136. https://doi.org/10.1111/j.1365-2362.2004.01302.x.
Saneyasu, T., Akhtar, R., Sakai, T., 2016. Molecular cues guiding matrix stiffness in liver fibrosis. Biomed Res. Int. 2016, 2646212. https://doi.org/10.1155/2016/2646212.
Sautot, P., et al., 2011. Structural, hydration, and phase transition properties of phosphatidylcholine from salmon heads. Eur. J. Lipid Sci. Technol. 113, 744–755. https://doi.org/10.1002/ejlt.201000449.
Schindelin, J., et al., 2012. Fiji: An open-source platform for biological-image analysis. Nat. Methods 9, 676–682. https://doi.org/10.1038/nmeth.2019.
Seebacher, F., Zeigerer, A., Kory, N., Krahmer, N., 2020. Hepatic lipid droplet homeostasis and fatty liver disease. Seminars in Cell & Developmental Biology 108, 72–81. https://doi.org/10.1016/j.semcdb.2020.04.011.
Tan, A., Rao, S., Prestidge, C.A., 2013. Transforming lipid-based oral drug delivery systems into solid dosage forms: An overview of solid carriers, physicochemical properties, and biopharmaceutical performance. Pharm. Res. 30, 2993–3017. https://doi.org/10.1007/s11095-013-1107-3.
Thoorens, G., Krier, F., Leclercq, B., Carlin, B., Evrard, B., 2014. Microcrystalline cellulose, a direct compression binder in a quality by design environment–a review. Int. J. Pharm. 473, 64–72. https://doi.org/10.1016/j.ijpharm.2014.06.055.
Trache, D., et al., 2016. Microcrystalline cellulose: Isolation, characterization and bio-composites application-A review. Int. J. Biol. Macromol. 93, 789–804. https://doi.org/10.1016/j.ijbiomac.2016.09.056.
Trombetta-Esilva, J., Bradshaw, A.D., 2012. The function of SPARC as a mediator of fibrosis. Open Rheumatol. J. 6, 146–155. https://doi.org/10.2174/1874312901206010146.
Tso, P., Balint, J.A., 1986. Formation and transport of chylomicrons by enterocytes to the lymphatics. Am. J. Phys. Anthropol. 250, G715–G726. https://doi.org/10.1152/ajpgi.1986.250.6.G715.
Tso, P., Lindstrom, M.B., Borgstrom, B., 1987. Factors regulating the formation of chylomicrons and very-low-density lipoproteins by the rat small intestine. Biochim. Biophys. Acta 922, 304–313. https://doi.org/10.1016/0005-2760(87)90053-1.
Valentino, G., Zivko, C., Weber, F., Brulisauer, L., Luciani, P., 2019. Synergy of phospholipid-drug formulations significantly deactivates profibrogenic human hepatic stellate cells. Pharmaceutics 11, 676. https://doi.org/10.3390/pharmaceutics11120676.
van Hoogevest, P., 2017. An update on the use of oral phospholipid excipients. Eur. J. Pharm. Sci. 108, 1–12. https://doi.org/10.1016/j.ejps.2017.07.008.
van Hoogevest, P., Wendel, A., 2014. The use of natural and synthetic phospholipids as pharmaceutical excipients. Eur. J. Lipid Sci. Technol. 116, 1088–1107. https://doi.org/10.1002/ejlt.201400219.
Varganova, D.L., Pavlov, C.S., Casazza, G., Nikolova, D., Gluud, C., 2019. Essential phospholipids for people with non-alcoholic fatty liver disease. Cochrane Database Syst. Rev. https://doi.org/10.1002/14651858.cd013301.
Wang, J., Ding, Y., Zhou, W., 2020. Albumin self-modified liposomes for hepatic fibrosis therapy via SPARC-dependent pathways. Int. J. Pharm. 574, 118940. https://doi.org/10.1016/j.ijpharm.2019.118940.
Xu, L., et al., 2005. Human hepatic stellate cell lines, LX-1 and LX-2: new tools for analysis of hepatic fibrosis. Gut 54, 142–151. https://doi.org/10.1136/gut.2004.042127.
Zivko, C., Fuhrmann, K., Fuhrmann, G., Luciani, P., 2022. Tracking matricellular protein SPARC in extracellular vesicles as a non-destructive method to evaluate lipid-based antifibrotic treatments. Commun Biol 5, 1155. https://doi.org/10.1038/s42003-022-04123-z.
Zivko, C., Witt, F., Koeberle, A., Fuhrmann, G., Luciani, P., 2023. Formulating elafibranor and obeticholic acid with phospholipids decreases drug-induced

association of SPARC to extracellular vesicles from LX-2 human hepatic stellate cells. Eur. J. Pharm. Biopharm. 182, 32–40. https://doi.org/10.1016/j.ejpb.2022.11.025.